Andreev transport in a correlated ferromagnet-quantum-dot-superconductor device

I. Weymann* and K. P. Wójcik
Faculty of Physics, Adam Mickiewicz University, ulica Umultowska 85, 61-614 Poznań, Poland
(Received 13 October 2015; published 14 December 2015)

The spin-resolved Andreev reflection processes in a hybrid ferromagnet-quantum-dot-superconductor device are theoretically studied. In particular, the transport coefficients, such as the Andreev transmission as well as the linear-response Andreev conductance, are calculated by means of the numerical renormalization group method. It is shown that, generally, transport properties are conditioned by the interplay of correlations leading to the Kondo effect, superconducting proximity effect, and ferromagnetic-contact-induced exchange field. The exchange field is shown to greatly affect the low-energy behavior of the Andreev transmission by splitting the Kondo resonance. Moreover, it leads to a nonmonotonic dependence of the Andreev conductance on the dot level position. At low temperatures, the conductance has a peak at the particle-hole symmetry point, which however becomes quickly suppressed with increasing the temperature. The mechanisms responsible for those effects are thoroughly discussed.

DOI: 10.1103/PhysRevB.92.245307 PACS number(s): 73.23.−b, 72.15.Qm, 74.45.+c, 72.25.−b

I. INTRODUCTION

Transport properties of hybrid quantum dot systems, involving both superconducting and normal electrodes, have recently been extensively studied both theoretically [1–28] and experimentally [29–34]. In such systems, at sufficiently low temperatures, the physics is determined by an interplay between the superconducting proximity effect and the correlations leading to the Kondo effect [35–38]. For a magnetic impurity coupled to a superconductor, the existence of the Kondo phenomenon is conditioned by the relative ratio of the Kondo temperature T_K to the superconducting energy gap Δ [39–41]. The Kondo phenomenon is present when $T_K > \Delta$. On the other hand, in the opposite situation when Δ exceeds T_K, the Kondo effect is suppressed and the so-called Yu-Shiba-Rusinov bound states form inside the energy gap [42–44]. Such proximity-induced bound states can be probed in a mesoscopic device consisting of a quantum dot, in which Andreev reflection [45] leads to the formation of similar long-lived states. In fact, Andreev bound states have been recently measured in bias spectroscopy experiments by attaching a second normal electrode to the dot acting as a weakly coupled probe [30–34]. However, when the coupling to the second electrode increases, such that the Kondo temperature associated with this normal reservoir becomes relevant, the system can again exhibit conductance enhancement due to the Kondo correlations. It was shown recently in the limit of large superconducting energy gap that, quite counterintuitively, in a hybrid normal-metal-quantum-dot-superconductor system increasing the strength of the coupling to superconducting electrode can lead to an enhancement of the Kondo temperature [26–28]. This is associated with the fact that the pairing correlations induced in the dot decrease the excitation energies to virtual states of the dot, leading to an increase in the effective exchange interaction, which consequently results in an increase of T_K.

An even more interesting situation occurs when the normal lead is ferromagnetic. Then, another energy scale becomes relevant, namely, the one associated with a spin-splitting of the dot level caused by the so-called effective exchange field [46–51]. When the exchange field is large enough, it can affect the Kondo state in a very considerable way by splitting or even fully suppressing the Kondo peak. The interplay of exchange field, Kondo, and proximity effects has been recently studied experimentally in a hybrid ferromagnet-quantum-dot-superconductor device [52]. It was shown that the coexistence of itinerant ferromagnetism with superconducting and Kondo correlations leads to a very complex differential conductance spectra, containing both signatures of subgap states and split Kondo resonance.

The main goal of this paper is to provide further insight into Andreev transport properties of such systems. By employing the nonperturbative and very accurate numerical renormalization group (NRG) method [53–55], we determine transport due to Andreev reflection in the full parameter space, where both the Kondo correlations, superconducting proximity effect, and ferromagnet-induced exchange field coexist. We analyze the dot level and temperature dependence of the Andreev transmission coefficient and the associated linear-response conductance for various coupling strengths to both superconducting and normal leads. We show that generally the transport properties are conditioned by a subtle interplay of the aforementioned energy scales. In particular, for relatively weak couplings to superconducting electrode, the Kondo resonance becomes split due to the exchange field. However, with increasing the coupling strength, the proximity effect leads to an enhancement of T_K and the Kondo resonance becomes reinstated.

The paper is organized in the following way. Theoretical framework is presented in Sec. II, where we first describe the model Hamiltonian (Sec. II A), define the quantities of interest (Sec. II B), and briefly describe the method used in calculations (Sec. II C). The main part of the paper is presented in Sec. III, in which we first describe the behavior of the local density of states of the dot (Sec. III A) and then analyze the Andreev transmission and the linear-response conductance (Sec. III B). Finally, the conclusions are given in Sec. IV.

*weymann@amu.edu.pl

II. THEORETICAL DESCRIPTION

A. Effective Hamiltonian

The schematic of the system is shown in Fig. 1. It consists of a quantum dot coupled to one ferromagnetic (FM) and one s-wave superconducting (SC) lead. Since in this paper we are mainly interested in the Andreev reflection processes, we consider the superconducting energy gap Δ to be the largest energy scale in the problem. In such a case, the system can be described by the following effective Hamiltonian [56]:

$$H = H_{\rm QD}^{\rm eff} + H_{\rm F} + H_{\rm TF}, \tag{1}$$

where

$$H_{\rm QD}^{\rm eff} = \sum_{\sigma} \varepsilon d_{\sigma}^{\dagger} d_{\sigma} + U d_{\uparrow}^{\dagger} d_{\uparrow} d_{\downarrow}^{\dagger} d_{\downarrow} + \Gamma_S (d_{\uparrow}^{\dagger} d_{\downarrow}^{\dagger} + d_{\downarrow} d_{\uparrow}). \tag{2}$$

Here, $d_{\sigma}^{\dagger}$ creates a spin-σ electron of energy ε in the quantum dot and U is the correlation energy between two electrons occupying the dot. The last term takes into account the creation and annihilation of Cooper pairs in the superconductor, the degrees of freedom of which were integrated out in the limit of $\Delta \to \infty$, where Γ_S denotes the strength of the coupling between the SC lead and the quantum dot [56]. The electrons in the ferromagnetic lead are modeled as noninteracting particles, $H_{\rm F} = \sum_{\mathbf{k}\sigma} \varepsilon_{\mathbf{k}\sigma} c_{\mathbf{k}\sigma}^{\dagger} c_{\mathbf{k}\sigma}$, with $c_{\mathbf{k}\sigma}^{\dagger}$ being the creation operator of a spin-σ electron with momentum $\mathbf{k}$ and energy $\varepsilon_{\mathbf{k}\sigma}$. The last term of the Hamiltonian, $H_{\rm TF}$, describes tunneling processes between the FM lead and the quantum dot. It is given by $H_{\rm TF} = \sum_{\mathbf{k}\sigma} V_{\mathbf{k}\sigma} (d_{\sigma}^{\dagger} c_{\mathbf{k}\sigma} + c_{\mathbf{k}\sigma}^{\dagger} d_{\sigma})$, where $V_{\mathbf{k}\sigma}$ denotes the tunnel matrix elements between the dot and the ferromagnet, which are assumed to be energy independent. The coupling to the FM lead gives rise to the broadening of the dot level, the half width of which is given by $\Gamma = (\Gamma^{\uparrow} + \Gamma^{\downarrow})/2$. Assuming the flat density of states of width $2D$, with $D \equiv 1$ used as energy unit, the spin-dependent coupling strength is given by $\Gamma^{\sigma} = \pi |V_{\sigma}|^2/2$. It can be further expressed in terms of the spin polarization $p = (\Gamma^{\uparrow} - \Gamma^{\downarrow})/(\Gamma^{\uparrow} + \Gamma^{\downarrow})$ of the FM lead as $\Gamma^{\sigma} = (1 \pm p)\Gamma$ [46,48,50].

The effective quantum dot Hamiltonian (2) is not diagonal in the local basis spanned by the following four states: $|0\rangle$, $|\sigma\rangle$, $|d\rangle$, for empty, singly occupied with spin σ and doubly occupied dot. However, it can be easily diagonalized and its eigenstates are $|\sigma\rangle$, $|+\rangle$, $|-\rangle$, where

$$|\pm\rangle = \frac{1}{\sqrt{2}} \left(\sqrt{1 \mp \frac{\delta}{\sqrt{\delta^2 + \Gamma_S^2}}}\, |0\rangle \pm \sqrt{1 \pm \frac{\delta}{\sqrt{\delta^2 + \Gamma_S^2}}}\, |d\rangle \right), \tag{3}$$

and $\delta = \varepsilon + U/2$ denotes the detuning from the particle-hole symmetry point of the dot. On the other hand, the energies of the above states are correspondingly given by $E_{\pm} = \delta \pm \sqrt{\delta^2 + \Gamma_S^2}$. The excitation energies of the effective dot Hamiltonian $H_{\rm QD}^{\rm eff}$ result in the following Andreev bound-state energies [16,18,25,26]:

$$E_{\alpha\beta}^{A} = \alpha \frac{U}{2} + \beta \sqrt{\delta^2 + \Gamma_S^2}, \tag{4}$$

with $\alpha, \beta = \pm$.

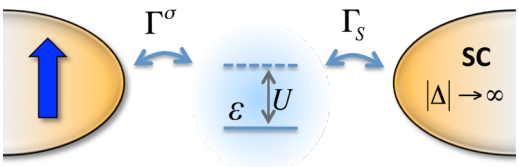

FIG. 1. (Color online) Schematic of the considered system. A single-level quantum dot is coupled to a ferromagnetic and superconducting (SC) lead with coupling strengths Γ^{σ} and Γ_S, respectively. The dot level energy is denoted by ε, while U is the Coulomb correlation energy. The superconducting energy gap Δ is assumed to be the largest energy scale in the problem, so that the only tunneling processes are exclusively due to the Andreev reflection.

B. Andreev transmission and conductance

The transmission coefficient for Andreev processes between the ferromagnetic and superconducting lead is given by [2,4,5,11]

$$T_A(\omega) = \sum_{\sigma} 4\Gamma^{\sigma}\Gamma^{\bar{\sigma}} \left| \langle\langle d_{\sigma} | d_{\bar{\sigma}} \rangle\rangle_{\omega}^{r} \right|^2, \tag{5}$$

where $\langle\langle d_{\sigma} | d_{\bar{\sigma}} \rangle\rangle_{\omega}^{r}$ is the Fourier transform of the corresponding off-diagonal retarded Green's function, $\langle\langle d_{\sigma} | d_{\bar{\sigma}} \rangle\rangle_{t}^{r} = -i\Theta(t)\langle\{d_{\sigma}(t), d_{\bar{\sigma}}(0)\}\rangle$. The linear-response Andreev conductance can be then found from [2,4,5,11]

$$G_A = \frac{2e^2}{h} \int d\omega\, T_A(\omega) \left(-\frac{\partial f(\omega)}{\partial \omega} \right), \tag{6}$$

with $f(\omega)$ denoting the Fermi-Dirac distribution function.

C. Calculation method

Because all the relevant linear-response transport coefficients are expressed in terms of the transmission coefficient, $T_A(\omega)$, the main task is to calculate its full energy and dot level detuning dependence. To perform this task in the most accurate manner, we employ the numerical renormalization group method [53–55]. Within this method the conduction band of FM lead is described by a tight-binding chain with exponentially decaying hoppings, which allows one to diagonalize the Hamiltonian iteratively and to find its full many-body eigenstates and eigenenergies. These can then be used to calculate any expectation value of both static and dynamic observables. Since in calculations it is crucial to keep a large number of states at each iteration, it is of vital importance to exploit as many symmetries the Hamiltonian possesses as possible. However, in the present problem, due to the superconducting pairing term in the effective Hamiltonian [cf. Eq. (2)] and the spin dependence of tunneling processes, only the zth component of the total spin is conserved, which makes the calculations challenging. In particular, here we kept $N_K = 4^6$ states at each iteration, exploiting one Abelian symmetry for the total spin zth component, and used the band discretization parameter $\Lambda = 2$. To find the Andreev transmission coefficient, we first determined the imaginary part of relevant Green's functions and then, from the

Kramers-Kronig relation, calculated the respective real parts. To obtain most reliable spectral functions from discrete NRG data, we employed the optimal broadening method [57] and used a z-averaging trick [58], averaging over two different discretizations.

III. RESULTS AND DISCUSSION

In this section we present and discuss the transport properties of the quantum dot connected to superconducting and ferromagnetic leads. We first study the behavior of the dot's local density of states in the Kondo regime on the strength of the coupling to superconducting lead. In particular, we analyze how the Kondo temperature T_K changes when Γ_S increases. Then, we study the detuning dependence of the Andreev transmission coefficient and the linear conductance for different temperatures, different coupling strengths, and spin polarization of the ferromagnetic lead.

A. Local density of states and the Kondo temperature

The local density of states of the dot is represented by the normalized spectral function $\pi\Gamma A(\omega) \equiv \sum_\sigma \pi\Gamma^\sigma A_\sigma(\omega)$, with $A_\sigma(\omega) = -(1/\pi)\mathrm{Im}\,\langle\langle d_\sigma | d_\sigma^\dagger\rangle\rangle^r_\omega$ and $\langle\langle d_\sigma | d_\sigma^\dagger\rangle\rangle^r_\omega$ being the Fourier transform of $\langle\langle d_\sigma | d_\sigma^\dagger\rangle\rangle^r_t = -i\Theta(t)\langle\{d_\sigma(t), d_\sigma^\dagger(0)\}\rangle$. Figure 2 presents the energy dependence of the normalized dot's level spectral function for different couplings to the superconducting lead Γ_S, as indicated. The spectral function is calculated both in the absence and presence of detunig, i.e., for $\varepsilon/U = -0.5$ ($\delta/U = 0$) and for $\varepsilon/U = -0.495$ ($\delta/U = 0.005$) Note that, in principle, in the case of the ferromagnetic lead the Kondo effect is generally suppressed due to the presence of ferromagnetic-contact-induced exchange field $\Delta\varepsilon_{\mathrm{exch}}$. Such an exchange field splits the dot levels, removing thus the degeneracy of the ground state, and the Kondo effect becomes destroyed when $|\Delta\varepsilon_{\mathrm{exch}}| \gtrsim T_K$ [46,47,49,51]. However, the exchange field has this special property that it vanishes at the particle-hole symmetry point $\delta = 0$. This is why in Fig. 2(a) the signatures of the Kondo effect are clearly visible, while in Fig. 2(b) the Kondo effect for small Γ_S is suppressed.

Let us first discuss the former case. When $\Gamma_S = 0$, the spectral function exhibits the Kondo-Abrikosov-Suhl resonance at the Fermi energy due to the Kondo effect, where $\pi\Gamma A(0) = 1$ [36]. When the coupling to the superconducting lead increases, the excitation energies between the singly occupied states and the states $|+\rangle$ and $|-\rangle$ decrease. As a result, the effective exchange interaction between the dot and the normal lead is increased, and so is the Kondo temperature [28]. This behavior can be clearly seen in Fig. 2(a). Moreover, when Γ_S is relatively large, the height of the resonance becomes diminished. This is associated with the fact that for $\Gamma_S = U/2$, all the dot's states become degenerate and the system is truly in the mixed-valence regime, so that the Kondo effect is absent.

For the considered hybrid device, by performing the Schrieffer-Wolff transformation, one can find the effective exchange interaction between the dot and the ferromagnetic lead, which then allows one to estimate the Kondo temperature

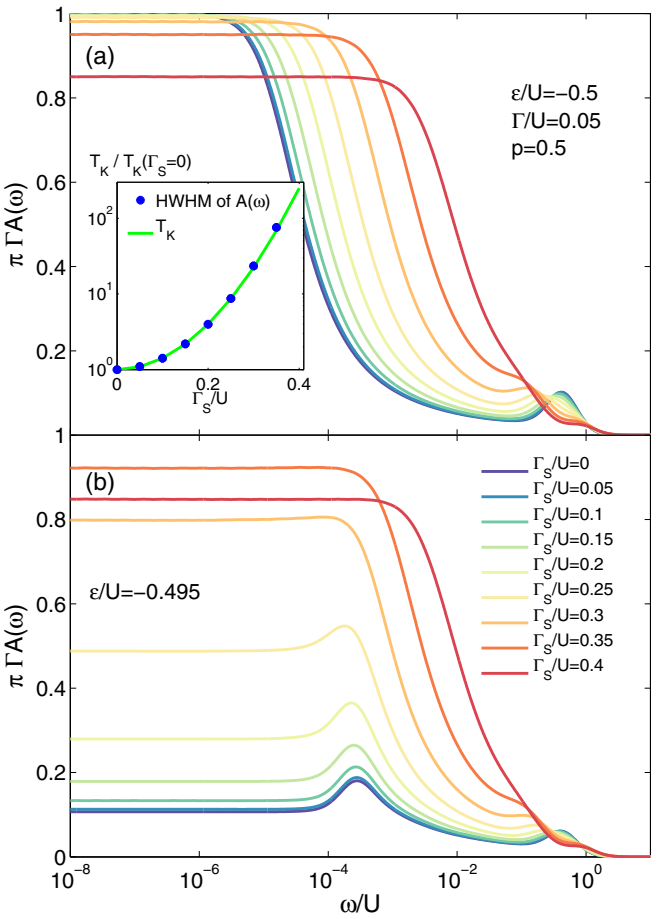

FIG. 2. (Color online) The normalized spectral function of the dot level, $\pi\Gamma A(\omega)$, as a function of energy ω for different coupling strengths to the superconductor Γ_S calculated for (a) $\delta/U = 0$ and (b) $\delta/U = 0.005$. The inset in (a) shows the Γ_S dependence of the Kondo temperature extracted from the half width at half maximum (HWHM) of the spectral function (points) and the fit as obtained from Eq. (7) with $\eta \approx 1.5$. The parameters are $U/D = 0.1$, $\Gamma/U = 0.05$, $T = 0$, and $p = 0.5$. Note the logarithmic energy scale.

[27,28,59],

$$T_K = \eta\sqrt{\frac{\Gamma U}{2}}\,\exp\left\{\frac{\pi\left[\varepsilon(\varepsilon+U)+\Gamma_S^2\right]}{2\Gamma U}\,\frac{\mathrm{arctanh}(p)}{p}\right\}, \quad (7)$$

with η being a constant of the order of unity. From the above formula it clearly follows that increasing Γ_S raises T_K. Moreover, in the case of ferromagnetic lead and in the absence of exchange field, the Kondo temperature is decreased by a spin polarization dependent factor [46]. The Kondo temperature estimated from the half width at half maximum (HWHM) of the spectral function plotted as a function of Γ_S is shown as bullets in the inset to Fig. 2(a). Clearly, the Kondo temperature rises with increasing the strength of the coupling to the superconducting lead. For comparison, the solid line in the inset shows the Kondo temperature obtained by using Eq. (7). The agreement with numerical data is indeed very good and the numerical constant was found to be $\eta \approx 1.5$.

In the case of finite detuning from the particle-hole symmetry point, the Kondo effect is generally suppressed.

Figure 2(b) shows the spectral function calculated for such δ that for assumed parameters the exchange field is slightly larger than T_K. In this situation the interplay of relevant energy scales is clearly visible. When $\Gamma_S = 0$, the Kondo resonance is suppressed since $|\Delta\varepsilon_{\rm exch}| > T_K$. However, when increasing the pairing correlations with Γ_S, the Kondo temperature rises and, once $T_K \gtrsim |\Delta\varepsilon_{\rm exch}|$, the Kondo peak becomes restored; see, e.g., the curves for larger Γ_S in Fig. 2(b). Further increase of the coupling to the superconductor eventually kills the Kondo effect, since the system enters the mixed-valence regime.

B. Andreev transmission and conductance

1. *Dependence on the coupling strength* Γ

The Andreev transmission coefficient plotted as a function of energy ω and dot level detuning δ is shown in Fig. 3 for different values of the coupling to the normal lead Γ. The left column corresponds to the case of a nonmagnetic lead, while the right column presents the case when the lead is ferromagnetic. The dashed lines show the energy of respective Andreev bound states; cf. Eq. (4). In the case of a nonmagnetic lead and when the coupling is small, $T_A(\omega)$ exhibits narrow peaks around the energies corresponding to resonances between the bound states, which occur for $\delta = \pm\sqrt{U^2/4 - \Gamma_S^2}$.

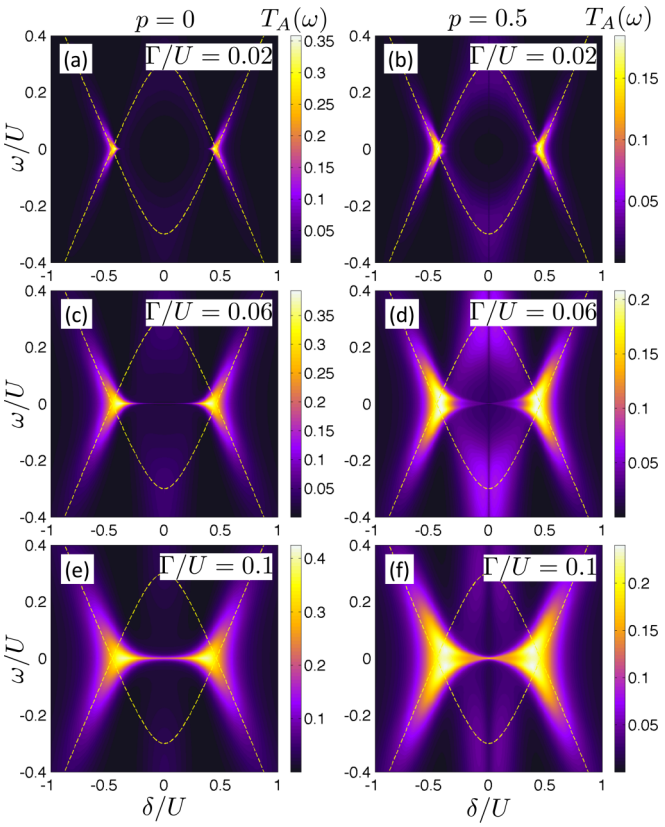

FIG. 3. (Color online) The Andreev transmission coefficient $T_A(\omega)$ as a function of energy ω and dot level detuning $\delta = \varepsilon + U/2$ in the case of nonmagnetic (left column, $p = 0$) and ferromagnetic (right column, $p = 0.5$) lead calculated for different couplings to normal lead Γ, as indicated in the figure. The dashed line shows the Andreev bound-state energies obtained from Eq. (4). The parameters are $U/D = 0.1$, $\Gamma_S/U = 0.2$, and $T = 0$.

However, with increasing Γ, the width of those peaks increases and, in addition, an extra resonance at $\omega = 0$ develops for $|\delta| \lesssim \sqrt{U^2/4 - \Gamma_S^2}$; see Fig. 3(e). In this transport regime the dot is singly occupied and the resonance in $T_A(\omega)$, which occurs at the Fermi energy, is due to the Kondo effect.

When the lead is ferromagnetic, the transmission coefficient is suppressed by approximately a factor of 2 as compared to the nonmagnetic case; see Fig. 3. This is due to the fact that transferring Cooper pairs between the superconductor and ferromagnet involves two electrons of opposite spins. While one of those electrons belongs to the spin-majority subband of ferromagnetic lead, the other one is a spin-minority electron. The density of states of minority carriers becomes then a bottleneck for Cooper pair transport [25,26].

While for detunings $|\delta| > \sqrt{U^2/4 - \Gamma_S^2}$, that is in the case when the dot occupancy is even, the behavior of $T_A(\omega)$ is similar to that in the case of $p = 0$; this is completely not the case when the dot is singly occupied, especially for larger Γ. First, one can see that transmission coefficient is enhanced in the singly occupied dot regime not only at low energies, but this enlargement extends to high energies, $|\omega| \approx U/2$. Second, the Kondo resonance is now split, which is most visible in the case of $\Gamma/U = 0.06$; see Fig. 3(d). This splitting is due to the proximity effect with a ferromagnetic lead, which results in the exchange field. If $|\Delta\varepsilon_{\rm exch}| \gtrsim T_K$, the Kondo resonance becomes suppressed and there are only side resonances occurring at $\omega = \pm\Delta\varepsilon_{\rm exch}$. Moreover, one can also see that the splitting of the zero-energy peak in $T_A(\omega)$ changes with δ. This is due to a particular dependence of $\Delta\varepsilon_{\rm exch}$ on the dot detuning: $\Delta\varepsilon_{\rm exch} = 0$ for $\delta = 0$ and it changes sign when δ crosses zero [26]. In fact, a similar split Kondo resonance has recently been observed experimentally in a ferromagnet-quantum-dot-superconductor device [52]. When the coupling to the normal lead increases, both T_K and $\Delta\varepsilon_{\rm exch}$ are enhanced. However, while $\Delta\varepsilon_{\rm exch}$ grows algebraically with Γ [26], T_K increases in an exponential way [36]; cf. Eq. (7). Consequently, for $\Gamma/U = 0.1$, the splitting of the Kondo resonance becomes obscured, see Fig. 3(f), since the condition $|\Delta\varepsilon_{\rm exch}| \gtrsim T_K$ is only very weakly satisfied.

From the transmission coefficient, by using Eq. (6), one can calculate the dot-level detuning dependence of the linear-response conductance. This is presented in Fig. 4, where the left (right) column corresponds to the nonmagnetic (ferromagnetic) case. Note the different scale for G_A in the left and right columns of the figure: the conductance for $p = 0.5$ is approximately two times smaller compared to that in the case of $p = 0$. When the coupling is relatively small, see the case for $\Gamma/U = 0.02$, the qualitative difference between the $p = 0$ and $p > 0$ cases is hardly visible. The linear conductance shows then only two resonant peaks for $\delta = \pm\sqrt{U^2/4 - \Gamma_S^2}$, the height of which becomes suppressed with increasing the temperature; see Figs. 4(a) and 4(b). However, for larger couplings between the dot and the normal lead, the differences become more pronounced. This is especially visible in the transport regime where the dot is singly occupied and the interplay of the exchange field and the correlations leading to the Kondo effect become essential.

First of all, one can see that the resonance peaks occurring for $\delta = \pm\sqrt{U^2/4 - \Gamma_S^2}$ become broadened when increasing the coupling strength Γ. Moreover, the low-temperature

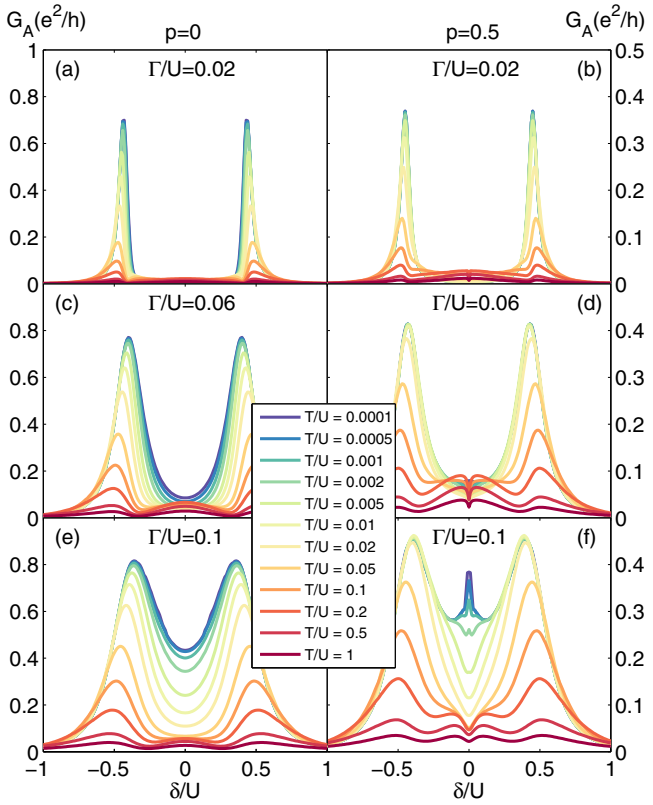

FIG. 4. (Color online) The detuning dependence of the linear-response conductance due to Andreev processes calculated for different temperatures T and couplings to normal lead Γ, as indicated. The left column corresponds to the case of $p = 0$, while the right column shows the case of $p = 0.5$. The parameters are the same as in Fig. 3. Note that the scale in the case of $p = 0.5$ is smaller by a factor of 2 compared to the case of $p = 0$.

conductance in the singly occupied regime, $-\sqrt{U^2/4 - \Gamma_S^2} < \delta < \sqrt{U^2/4 - \Gamma_S^2}$, rises with enhancing Γ. These two effects result simply from the fact that increasing Γ leads to broadening of the dot levels and to an increase of the Kondo temperature. It reveals as a gradual enhancement of the low-T conductance in the transport regime where the dot is singly occupied. This general tendency can be seen in the case of both nonmagnetic and ferromagnetic leads. However, there are important differences visible especially for $\Gamma/U = 0.1$; see Figs. 4(e) and 4(f). While in the case of a nonmagnetic lead, G_A in the Kondo valley rises rather uniformly with decreasing T; for a ferromagnetic lead, this enhancement is most pronounced for $\delta = 0$. In fact, when the dot level is detuned from the particle-hole symmetry point the conductance suddenly drops. This results in a peak in G_A as a function of δ, occurring for $\delta = 0$. When the temperature increases, however, this peak becomes smeared and disappears. The occurrence of this peak can be understood by invoking the relevant energy scales in this problem: T_K and $\Delta\varepsilon_{\text{exch}}$ (for fixed Γ_S). By detuning the dot level from $\delta = 0$, the exchange field becomes finite and increases with increasing $|\delta|$. Consequently, once δ is such that $|\Delta\varepsilon_{\text{exch}}| \gtrsim T_K$, the Kondo resonance becomes obscured and the conductance drops. In fact, the maximum value of G_A for $\delta = 0$ is comparable in both cases of $p = 0$ and $p = 0.5$; see Figs. 4(e) and 4(f). In the nonmagnetic case, however, G_A changes monotonically when moving away from $\delta = 0$ towards resonances, contrary to the ferromagnetic case, when G_A behaves in a nonmonotonic way.

2. *Dependence on the coupling strength* Γ_S

The Andreev transmission coefficient as a function of energy ω and dot level detuning δ for different couplings to superconducting lead Γ_S is shown in Fig. 5. Again, the right column presents the ferromagnetic lead case, while the left one, for comparison, corresponds to the nonmagnetic case. This figure illustrates how the transmission coefficient changes when Γ_S increases from low to high values, where for

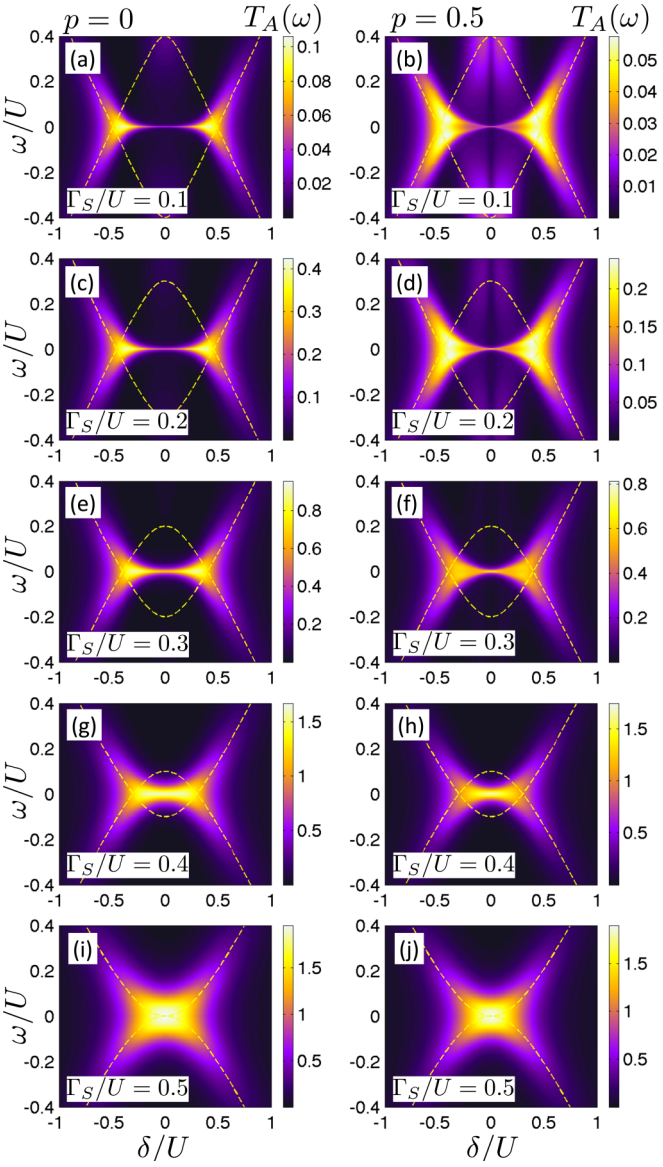

FIG. 5. (Color online) The Andreev transmission coefficient $T_A(\omega)$ as a function of energy ω and dot level detuning δ in the case of nonmagnetic (left column, $p = 0$) and ferromagnetic (right column, $p = 0.5$) lead for different couplings to superconducting lead Γ_S, as indicated in the figure. Parameters are the same as in Fig. 3 with $\Gamma/U = 0.1$.

$\Gamma_S = U/2$ the Kondo valley is absent and all Andreev bound states are at resonance for $\delta = 0$.

First, let us discuss a general tendency, which is visible irrespective of the spin polarization of the normal lead. When Γ_S increases, the resonances for $\delta = \pm\sqrt{U^2/4 - \Gamma_S^2}$ move towards the particle-hole symmetry point and merge when $\Gamma_S = U/2$. Increasing Γ_S is also associated with an enhancement of the Kondo temperature; cf. Eq. (7). As a consequence, once can see that the width of the Kondo peak slightly increases with Γ_S. However, for larger values of Γ_S, see, e.g., $\Gamma_S/U \gtrsim 0.4$, the Kondo peak gets merged with the two resonant peaks and only a single resonant peak occurs with $T_A(\omega) = 2$; see Figs. 5(i) and 5(j).

The difference between the ferromagnetic and nonmagnetic cases is most visible when the coupling to superconductor is relatively low; see the case of $\Gamma_S/U \lesssim 0.2$ in Fig. 5. For $\Gamma_S/U \lesssim 0.2$, one can clearly see the split Kondo resonance in the transmission coefficient. However, further increase of Γ_S decreases the ratio of $|\Delta\varepsilon_{\rm exch}|/T_{\rm K}$, such that the exchange field effects become suppressed and $T_A(\omega)$ shows the restored Kondo peak. (Note that $T_{\rm K}$ depends exponentially on Γ_S and increases with rising the coupling to the superconductor.) In other words, superconducting correlations win over the ferromagnetic contact proximity effects and the transmission coefficient for $\Gamma_S/U \gtrsim 0.3$ starts behaving very similarly in both the $p = 0$ and the finite-p case; see Fig. 5.

This tendency is also clearly visible in the detunig dependence of the linear conductance calculated for different temperatures and values of Γ_S corresponding to Fig. 5, which is shown in Fig. 6. In the nonmagnetic case, increasing Γ_S leads to an enhancement of the linear conductance, until it eventually reaches its maximum value, $G_A = 4e^2/h$, for $\delta = 0$ and $\Gamma_S = U/2$. Note that this value persists to relatively high temperatures and starts decreasing when $T/U \gtrsim 0.01$; see Fig. 6(i).

Comparing the left and right column of Fig. 6 reveals the nontrivial differences between the case of ferromagnetic and nonmagnetic leads. Moreover, the differences are now much better resolved compared to Fig. 5, especially at low temperatures. In the case of finite p, one can clearly see a resonant peak at $\delta = 0$ for $\Gamma_S/U \lesssim 0.3$. As mentioned above, this peak is associated with the fact that the exchange field vanishes at the particle-hole symmetry point and the Kondo peak develops, while it becomes suddenly suppressed at small but finite detuning. For larger couplings to superconducting lead, the superconducting proximity effects dominate, and the differences between the ferromagnetic and nonmagnetic cases are suppressed. Consequently, the detuning dependence of the conductance is then qualitatively the same in both cases, though small quantitative differences can still be observed; see Fig. 6.

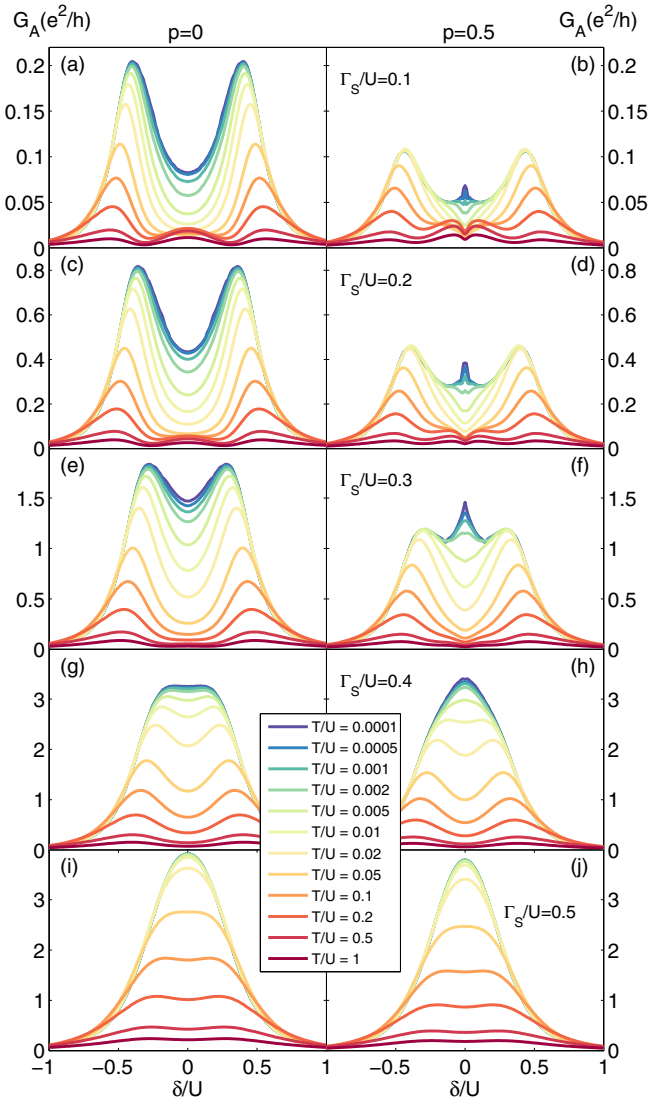

FIG. 6. (Color online) The detuning dependence of the linear conductance due to Andreev reflection for different temperatures. The left column corresponds to the case of $p = 0$, and the right column to the case of $p = 0.5$. Each row presents the results obtained for different coupling Γ_S, as indicated in the panels on the right-hand side. Parameters are the same as in Fig. 3 with $\Gamma/U = 0.1$.

3. *Dependence on the spin polarization p*

In the previous sections we have discussed the detuning dependence of both $T_A(\omega)$ and G_A when either Γ or Γ_S was varied. Now, we assume constant couplings and study how the Andreev transport properties depend on the degree of spin polarization of ferromagnetic lead. In other words, while approximately keeping the same superconducting parity correlations and correlations leading to the Kondo effect, we gradually increase the ferromagnetic proximity effects.

The corresponding detuning and energy dependence of the Andreev transmission coefficient is shown in Fig. 7, where each panel corresponds to different p, starting from $p = 0$ to $p = 0.9$. Two main features can be immediately noticed. First, increasing spin polarization leads to an overall suppression of $T_A(\omega)$. The reason for it has already been explained earlier and is related with the mismatch between the majority and minority subbands of the ferromagnet. Injecting or subtracting Cooper pairs involves two electrons of opposite spin, thus in an ideal case of a half metal, the Andreev reflection will be fully blocked. Second, the splitting of the Kondo peak with increasing p can be clearly visible. It can be seen that this splitting increases with increasing p, which is directly

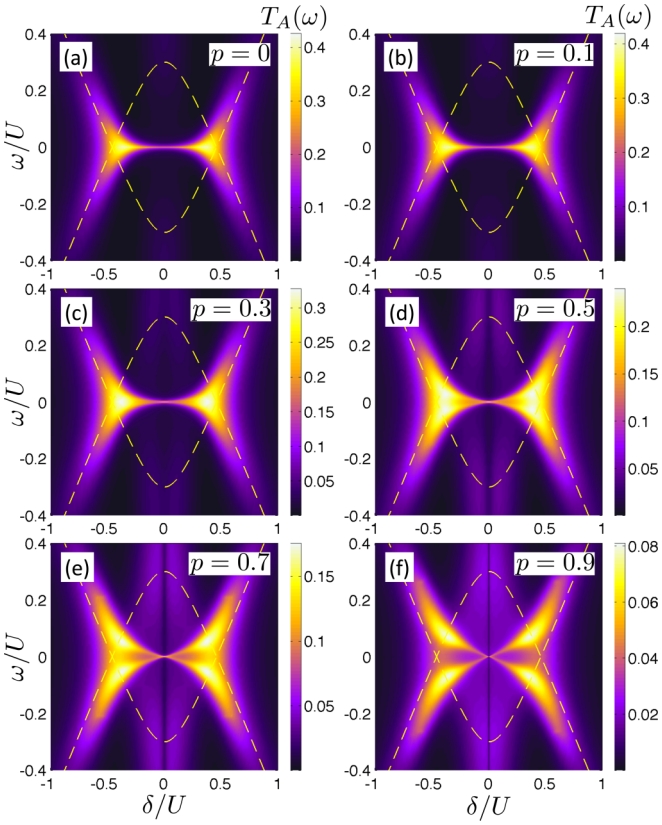

FIG. 7. (Color online) The energy and dot level detuning dependence of the Andreev transmission coefficient for different spin polarization p of ferromagnetic lead, as indicated. Parameters are the same as in Fig. 3 with $\Gamma/U = 0.1$ and $\Gamma_S/U = 0.2$.

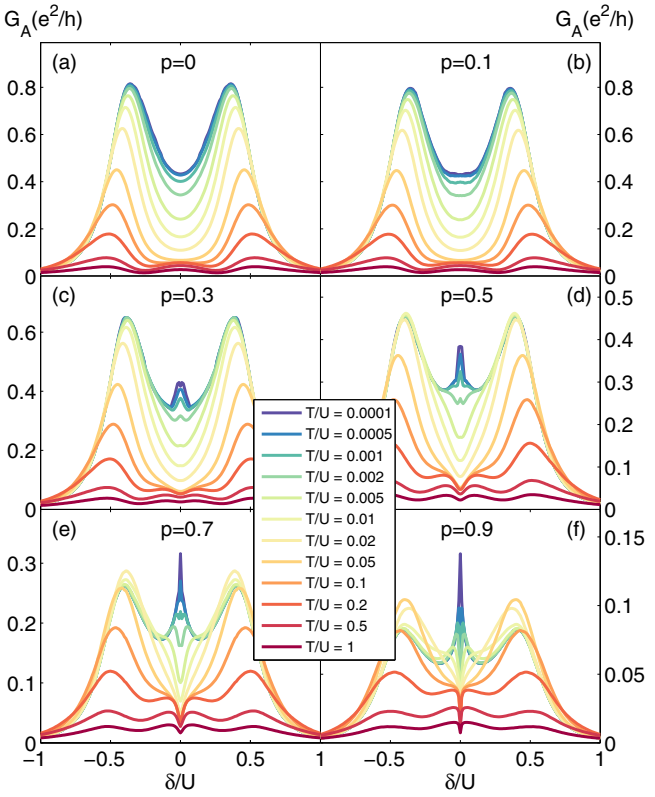

FIG. 8. (Color online) The dot level detuning dependence of the Andreev conductance for different temperatures and for different spin polarization p, as indicated. Parameters are the same as in Fig. 3 with $\Gamma/U = 0.1$ and $\Gamma_S/U = 0.2$.

associated with the fact that the magnitude of $\Delta\varepsilon_{\rm exch}$ grows with rising p [26].

Interestingly, one can also note that rising spin polarization p leads to an enhancement of $T_A(\omega)$ in the singly occupied regime for energies much larger than those corresponding to the split Kondo resonance. In fact, this enhancement can be seen in the whole range of energy ω considered in the figure, except for $\omega \approx 0$; see, e.g., Fig. 7(f). Moreover, a similar enhancement could be also observed in other figures presenting the energy and detunig dependence of $T_A(\omega)$; cf. Figs. 3(d) and 5(b). The maximum of $T_A(\omega)$ in this energy range occurs around the position of the Andreev bound states. Furthermore, although such enhancement of Andreev transmission occurs in both cases of ferromagnetic and nonmagnetic leads, it is more pronounced in the former case. This finding implies that ferromagnetic proximity effects are relevant not only at low-energy scales, of the order of $\Delta\varepsilon_{\rm exch}$ where they condition the occurrence of the Kondo effect, but they also play an important role at larger energy scales. This is in accordance with an observation that the exchange field can lead to a full spin polarization of the Hubbard resonances in the spectral function of the dot level, even when $|\Delta\varepsilon_{\rm exch}| \ll U$ [60].

Intuitively, the enhancement of the Andreev transmission for $p > 0$ can be explained as follows. For ferromagnetic lead the local density of states of the quantum dot $A_\sigma(\omega)$ becomes spin polarized at all energy scales. This polarization is such that if $A_\uparrow(\omega)$ is enhanced with respect to the $p = 0$ case, then $A_\downarrow(-\omega)$ is also enhanced, while $A_\downarrow(\omega)$ and $A_\uparrow(-\omega)$ are suppressed. Thus, the probability of finding a pair of electrons with opposite spins and energies increases. Consequently, in the case of ferromagnetic lead the Andreev transport becomes enhanced. However, one needs to keep in mind that since Andreev transmission is proportional to $(1 - p^2)\Gamma^2$, cf. Eq. (5), increasing the spin polarization of the ferromagnetic lead will eventually result in the suppression of $T_A(\omega)$.

The dependence of the linear conductance on the detuning parameter δ calculated for different spin polarization p and temperature T is shown in Fig. 8. When the spin polarization increases, the magnitude of the low-temperature Andreev conductance gets suppressed and a peak for $\delta = 0$ develops. The relative height of this peak increases with rising p. This is due to the fact that $\Delta\varepsilon_{\rm exch}$ grows with p [26]. When the temperature increases, the peak in G_A as a function of δ in the center of the Coulomb blockade becomes smeared out, since thermal fluctuations suppress the Kondo effect. Interestingly, at high temperatures the dependence of conductance on the parameter δ in the singly occupied dot regime again becomes nonmonotonic. G_A shows then a small minimum, which develops for $\delta = 0$; see Fig. 8. This minimum is associated with the fact that $T_A(\omega)$ in the case of a ferromagnetic lead is suppressed in a narrow region around $\delta = 0$ for energies larger than the Kondo temperature; see also Figs. 3(d), 5(b), and 7.

IV. CONCLUSIONS

In this paper we have studied the transport properties of a hybrid superconductor-quantum-dot-ferromagnet device, focusing on the Andreev reflection processes. The system was modeled by an effective Hamiltonian with an on-dot pairing term in the limit of large superconducting energy gap. The calculations were performed by using the numerical renormalization group method, employing the optimal broadening, and z-averaging tricks to obtain high quality spectral data for the determination of the Andreev transmission coefficient. Generally, all transport characteristics revealed a subtle interplay of the three important energy scales in the problem: the Kondo temperature, the superconducting pairing correlations, and the effective exchange field.

In particular, it was shown that the Andreev transmission exhibits the Kondo resonance in the singly occupied dot regime, which can be split by the exchange field. Moreover, a suppression of the Andreev transmission was found at the particle-hole symmetry point for energies larger than the Kondo temperature. These effects were also revealed in the dot level detuning dependence of the Andreev conductance for different temperatures. At low T, G_A showed a peak for $\delta = 0$ due to the Kondo effect, however, for larger temperatures this peak developed into a local minimum. Furthermore, the exchange-field effects were shown to dominate transport behavior by splitting the Kondo resonance for moderate couplings to the superconducting lead. With increasing the strength of this coupling, the ferromagnetic proximity effects were however becoming less and less important. This was associated with an increase of the Kondo temperature when increasing the superconducting pairing correlations, which led to a lowering of the relevant excitation energies and, thus, to an enhancement of the exchange interaction between the spin in the dot and spins of itinerant electrons.

ACKNOWLEDGMENTS

We acknowledge discussions with J. Barnaś and P. Trocha. This work was supported by the National Science Centre in Poland through the Project No. DEC-2013/10/E/ST3/00213 and Marie Curie FP-7-Reintegration-Grants (Grant No. CIG-303 689) within the 7th European Community Framework Programme.

[1] R. Fazio and R. Raimondi, Phys. Rev. Lett. **80**, 2913 (1998).
[2] Q.-F. Sun, J. Wang, and T.-H. Lin, Phys. Rev. B **59**, 3831 (1999).
[3] J. C. Cuevas, A. Levy Yeyati, and A. Martín-Rodero, Phys. Rev. B **63**, 094515 (2001).
[4] Y. Zhu, Q.-F. Sun, and T.-H. Lin, Phys. Rev. B **65**, 024516 (2001).
[5] J.-F. Feng and S.-J. Xiong, Phys. Rev. B **67**, 045316 (2003).
[6] Y. Avishai, A. Golub, and A. D. Zaikin, Phys. Rev. B **67**, 041301(R) (2003).
[7] M. Krawiec and K. I. Wysokiński, Supercond. Sci. Technol. **17**, 103 (2004).
[8] Y. Tanaka, N. Kawakami, and A. Oguri, J. Phys. Soc. Jpn. **76**, 074701 (2007).
[9] T. Domański, A. Donabidowicz, and K. I. Wysokiński, Phys. Rev. B **76**, 104514 (2007).
[10] J. Bauer, A. Oguri, and A. C. Hewson, J. Phys.: Condens. Matter **19**, 486211 (2007).
[11] T. Domański, A. Donabidowicz, and K. I. Wysokiński, Phys. Rev. B **78**, 144515 (2008).
[12] C. Karrasch, A. Oguri, and V. Meden, Phys. Rev. B **77**, 024517 (2008).
[13] T. Hecht, A. Weichselbaum, J. von Delft, and R. Bulla, J. Phys.: Condens. Matter **20**, 275213 (2008).
[14] C. Karrasch and V. Meden, Phys. Rev. B **79**, 045110 (2009).
[15] T. Meng, S. Florens, and P. Simon, Phys. Rev. B **79**, 224521 (2009).
[16] D. Futterer, M. Governale, M. G. Pala, and J. König, Phys. Rev. B **79**, 054505 (2009).
[17] V. Koerting, B. M. Andersen, K. Flensberg, and J. Paaske, Phys. Rev. B **82**, 245108 (2010).
[18] B. Sothmann, D. Futterer, M. Governale, and J. König, Phys. Rev. B **82**, 094514 (2010).
[19] B. M. Andersen, K. Flensberg, V. Koerting, and J. Paaske, Phys. Rev. Lett. **107**, 256802 (2011).
[20] K. I. Wysokiński, J. Phys.: Condens. Matter **24**, 335303 (2012).
[21] D. Futterer, J. Swiebodzinski, M. Governale, and J. König, Phys. Rev. B **87**, 014509 (2013).
[22] A. Oguri, Y. Tanaka, and J. Bauer, Phys. Rev. B **87**, 075432 (2013).
[23] J. Barański and T. Domański, J. Phys.: Condens. Matter **25**, 435305 (2013).
[24] K. Bocian and W. Rudziński, Eur. Phys. J. B **86**, 439 (2013).
[25] I. Weymann and P. Trocha, Phys. Rev. B **89**, 115305 (2014).
[26] K. P. Wójcik and I. Weymann, Phys. Rev. B **89**, 165303 (2014).
[27] R. Zitko, J. S. Lim, R. López, and R. Aguado, Phys. Rev. B **91**, 045441 (2015).
[28] T. Domański, I. Weymann, M. Barańska, and G. Górski (unpublished).
[29] R. S. Deacon, Y. Tanaka, A. Oiwa, R. Sakano, K. Yoshida, K. Shibata, K. Hirakawa, and S. Tarucha, Phys. Rev. Lett. **104**, 076805 (2010); Phys. Rev. B **81**, 121308(R) (2010).
[30] E. J. H. Lee, X. Jiang, R. Aguado, G. Katsaros, C. M. Lieber, and S. De Franceschi, Phys. Rev. Lett. **109**, 186802 (2012).
[31] J. D. Pillet, P. Joyez, R. Žitko, and M. F. Goffman, Phys. Rev. B **88**, 045101 (2013).
[32] E. J. H. Lee, X. Jiang, M. Houzet, R. Aguado, Ch. M. Lieber, S. De Franceschi, Nat. Nanotechnol. **9**, 79 (2014).
[33] J. Schindele, A. Baumgartner, R. Maurand, M. Weiss, and C. Schönenberger, Phys. Rev. B **89**, 045422 (2014).
[34] A. Kumar, M. Gaim, D. Steininger, A. Levy Yeyati, A. Martin-Rodero, A. K. Hüttel, and C. Strunk, Phys. Rev. B **89**, 075428 (2014).
[35] J. Kondo, Prog. Theor. Phys. **32**, 37 (1964).
[36] A. C. Hewson, *The Kondo Problem to Heavy Fermions* (Cambridge University Press, Cambridge, UK, 1993).
[37] D. Goldhaber-Gordon, H. Shtrikman, D. Mahalu, D. Abusch-Magder, U. Meirav, and M. A. Kastner, Nature (London) **391**, 156 (1998).
[38] S. Cronenwett, T. H. Oosterkamp, and L. P. Kouwenhoven, Science **281**, 540 (1998).

[39] S. De Franceschi, L. Kouwenhoven, C. Schönenberger, and W. Wernsdorfer, Nat. Nanotechnol. **5**, 703 (2010).
[40] A. Martín-Rodero and A. Levy-Yeyati, Adv. Phys. **60**, 899 (2011).
[41] Ch. Schoenenberger and R. Maurand, Physics **6**, 75 (2013).
[42] L. Yu, Acta Phys. Sin. **21**, 75 (1965).
[43] H. Shiba, Prog. Theor. Phys. **40**, 435 (1968).
[44] A. I. Rusinov, Zh. Eksp. Teor. Fiz. **56**, 2047 (1969) [Sov. Phys. JETP **29**, 1101 (1969)].
[45] A. F. Andreev, J. Exptl. Theoret. Phys. **46**, 1823 (1964) [Sov. Phys. JETP **19**, 1228 (1964)].
[46] J. Martinek, Y. Utsumi, H. Imamura, J. Barnaś, S. Maekawa, J. König, and G. Schön, Phys. Rev. Lett. **91**, 127203 (2003).
[47] A. N. Pasupathy, R. C. Bialczak, J. Martinek, J. E. Grose, L. A. K. Donev, P. L. McEuen, and D. C. Ralph, Science **306**, 86 (2004).
[48] M. Sindel, L. Borda, J. Martinek, R. Bulla, J. König, G. Schön, S. Maekawa, and J. von Delft, Phys. Rev. B **76**, 045321 (2007).
[49] J. Hauptmann, J. Paaske, and P. Lindelof, Nat. Phys. **4**, 373 (2008).
[50] I. Weymann, Phys. Rev. B **83**, 113306 (2011).
[51] M. Gaass, A. K. Hüttel, K. Kang, I. Weymann, J. von Delft, and Ch. Strunk, Phys. Rev. Lett. **107**, 176808 (2011).
[52] L. Hofstetter, A. Geresdi, M. Aagesen, J. Nygard, C. Schönenberger, and S. Csonka, Phys. Rev. Lett. **104**, 246804 (2010).
[53] K. G. Wilson, Rev. Mod. Phys. **47**, 773 (1975).
[54] R. Bulla, T. A. Costi, and T. Pruschke, Rev. Mod. Phys. **80**, 395 (2008).
[55] We used an open-access Budapest NRG code, http://www.phy.bme.hu/~dmnrg/; O. Legeza, C. P. Moca, A. I. Tóth, I. Weymann, and G. Zaránd, arXiv:0809.3143.
[56] A. V. Rozhkov and D. P. Arovas, Phys. Rev. B **62**, 6687 (2000).
[57] A. Freyn and S. Florens, Phys. Rev. B **79**, 121102(R) (2009).
[58] V. L. Campo and L. N. Oliveira, Phys. Rev. B **72**, 104432 (2005).
[59] M. M. Salomaa, Phys. Rev. B **37**, 9312 (1988).
[60] Sz. Csonka, I. Weymann, and G. Zarand, Nanoscale **4**, 3635 (2012).